Modification by SiO$_2$ of Alumina Support for Light Alkane Dehydrogenation Catalysts

Giyjaz E. Bekmukhamedov *, Alya N. Mukhamed'yarova, Svetlana R. Egorova and Alexander A. Lamberov

A. Butlerov Institute of Chemistry, Kazan Federal University, Kazan 420008, Russia; anm03@list.ru (A.N.M.); svetlana.egorova@kpfu.ru (S.R.E.); alexander.lamberov@kpfu.ru (A.A.L.)

* Correspondence: gbekmouk@kpfu.ru; Tel.: +7-843-231-5346

Abstract: Due to the continuously rising demand for C$_3$–C$_5$ olefins it is important to improve the performance of catalysts for dehydrogenation of light alkanes. In this work the effect of modification by SiO$_2$ on the properties of the alumina support and the chromia-alumina catalyst was studied. SiO$_2$ was introduced by impregnation of the support with a silica sol. To characterize the supports and the catalysts the following techniques were used: low-temperature nitrogen adsorption; IR-spectroscopy; magic angle spinning ^{29}Si nuclear magnetic resonance; temperature programmed desorption and reduction; UV-Vis-, Raman- and electron paramagnetic resonance (EPR)-spectroscopy. It was shown that the modifier in amounts of 2.5–7.5 wt % distributed on the support surface in the form of SiO$_x$-islands diminishes the interaction between the alumina support and the chromate ions (precursor of the active component). As a result, polychromates are the compounds predominantly stabilized on the surface of the modified support; under thermal activation of the catalyst and are reduced to the amorphous Cr$_2$O$_3$. This in turn leads to an increase in the activity of the catalyst in the dehydrogenation of isobutane.

Keywords: alumina support; chromia-alumina catalyst; silica; isobutane dehydrogenation

1. Introduction

Catalysts with surface chromium species as an active component have large practical importance and are widely used in industrial organic synthesis. Microspherical chromia-alumina catalysts for alkane dehydrogenation in terms of consumption hold the leading position in the petrochemical industry of Russia [1]. This process is intended for production of C$_3$–C$_5$-olefin which is the raw material for synthesis of rubbers, plastics, synthetic films and filaments, high-octane components of fuel, etc. [2].

There are two methods of microspherical chromia-alumina catalysts preparation: the mixing of precursors of the support and active component followed by spray drying of the slurry obtained [3]; and the impregnation of the support by the solutions of the active component and the promoter. The catalysts obtained by the first method have a low mechanical strength under the conditions of a fluidized bed and the continuous circulation between the reactor and regenerator [4]. The method of support impregnation seems the most promising. Earlier a method of a gibbsite transformation to boehmite (precursor of γ-Al$_2$O$_3$) in the volume of the microgranule by a sequential thermal and hydrothermal treatment was developed [5]. The support obtained that way has a high mechanical strength, middle porosity, and a low surface acidity.

Continuously rising demand for light olefins [2,6] as well as the increase in the cost of natural energy resources requires high active and selective catalysts. It is possible to improve the catalyst performance by introduction of the modifiers. The modifiers of chromia dehydrogenation catalyst

SiO$_2$ [7], ZrO$_2$ [8–10], lanthanum [10,11], tin [7,12] and cerium [13] are usually used. Among these modifiers SiO$_2$ is the most accessible and inexpensive; its use is broadly described in the patent literature [14]. However, the mechanism of its positive effect on the performance of the dehydrogenation catalyst has not been described in detail. Therefore, in this article we studied the effect of modification of the structure and properties of the novel alumina support and chromia-alumina catalyst by SiO$_2$.

2. Results and Discussion

2.1. Alumina Support

2.1.1. Thermal Treatment of Boehmite Precursor

The microspherical support was used as a precursor of alumina (Figure 1). It was obtained according to the Scheme 1 [5]:
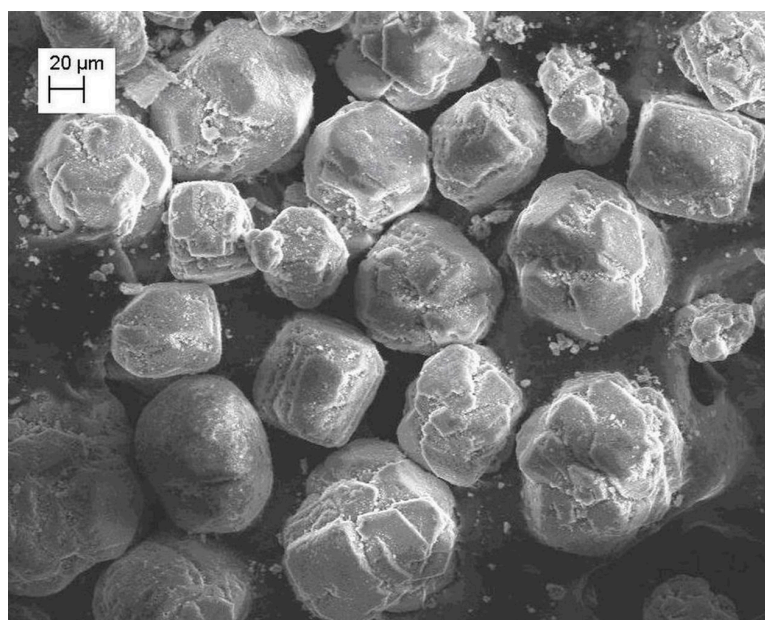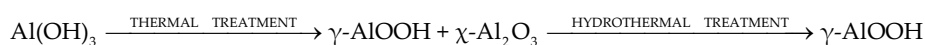

Figure 1. Scanning electron microscopy (SEM) image of the microspherical support.

$$Al(OH)_3 \xrightarrow{\text{THERMAL TREATMENT}} \gamma\text{-AlOOH} + \chi\text{-Al}_2\text{O}_3 \xrightarrow{\text{HYDROTHERMAL TREATMENT}} \gamma\text{-AlOOH}$$

Scheme 1. Production of alumina precursor.

According to the X-ray diffraction (Figure 2), the alumina precursor is a well-crystallized boehmite with crystallite size $D_{(020)}$ = 44 nm and $D_{(120)}$ = 47 nm. A high degree of boehmite crystallinity causes its small specific surface area (S_{BET}) and pore volume (V_p) = 27 m$^2 \cdot$g^{-1} and 0.07 cm$^3 \cdot$g^{-1} respectively (Table 1).

The choice of the boehmite thermal treatment temperature was made based on changes in the specific surface area and the number of strong acid sites (with the energy of ammonia desorption $E_{\text{des.NH}_3}$ more than 150 kJ$\cdot$mol^{-1}) obtained in alumina (Table 1). It is known that strong acid sites are active in hydrocarbon cracking reactions [15,16].

Thermal treatment of the precursor at 750 °C leads to the formation of mesopores (Figure 3), an increase in the specific surface area up to 92 m$^2 \cdot$g^{-1} and in the pore volume up to 0.27 cm$^3 \cdot$g^{-1} as a result of dehydration and the phase transition of boehmite to γ-Al$_2$O$_3$ (Figure 2). An increase of treatment temperature to 850 °C resulted in the decrease of the specific surface area to 62 m$^2 \cdot$g^{-1} due to pore enlargement (Table 1).
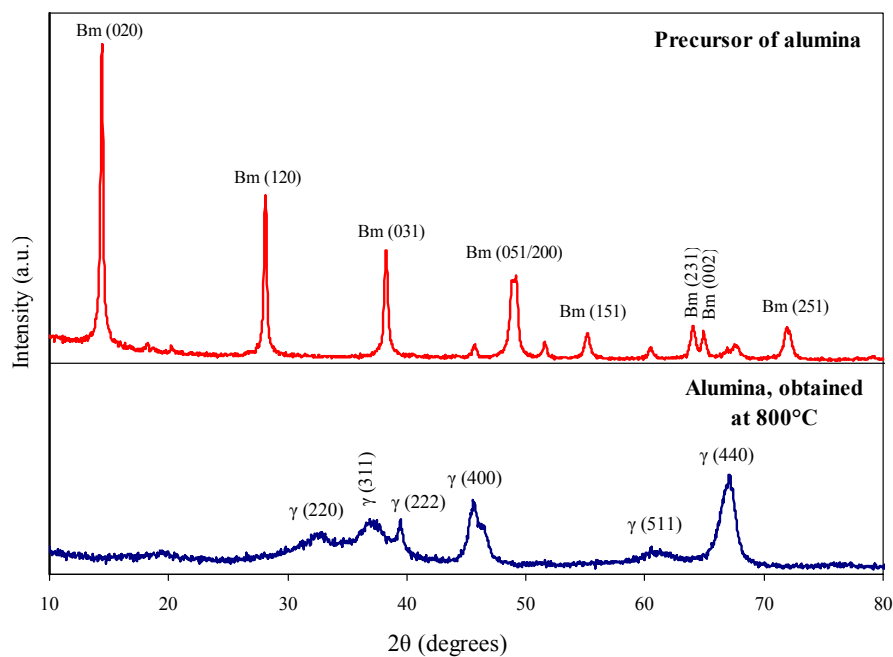
Figure 2. X-ray diffraction patterns of precursor of alumina and alumina support, obtained at 800 °C.

Table 1. Integral parameters of the porous system and the acidity of alumina supports.

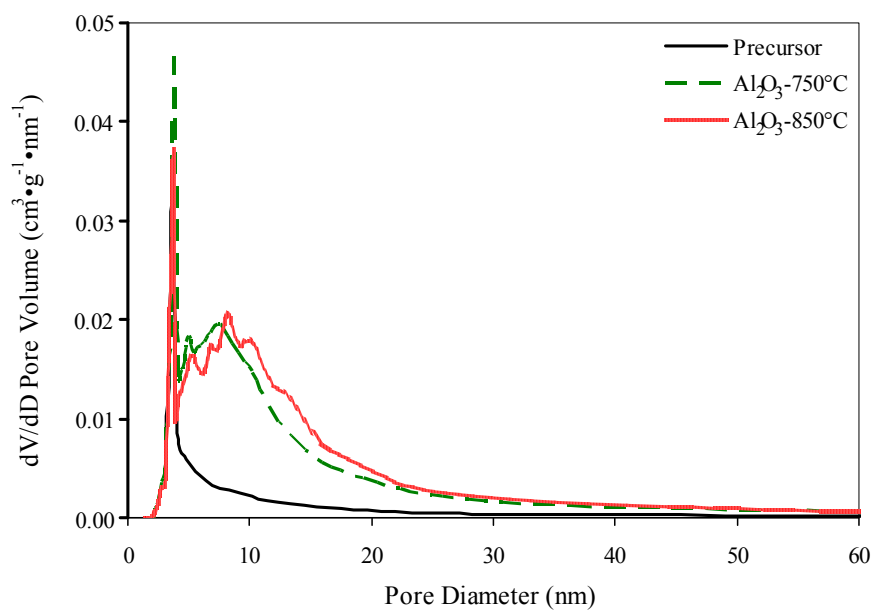| Sample	Temperature of Treatment	Crystalline Phase	Brunauer-Emmett-Teller (BET) Surface Area $(m^2 \cdot g^{-1})$	Pore Volume $(cm^3 \cdot g^{-1})$	Total Number of Acid Sites $(\mu mol \cdot g^{-1})$	Number of Acid Sites with $E_{des.NH_3} > 150$ $kJ \cdot mol^{-1}$ $(\mu mol \cdot g^{-1})$
Precursor of Alumina	-	γ-AlOOH	27	0.07	-	-
Alumina support	750 800 850	γ-Al$_2$O$_3$	92 83 62	0.27 0.26 0.26	125.8 102.3 91.8	16.2 10.0 8.5

Figure 3. Pore size distribution for precursor of alumina and alumina supports, obtained at 750 °C and 850 °C.

It is also accompanied by a decrease in the number of strong acid sites due to the reduction of the support surface, its dehydroxylation, as well as the transformation of the crystal structure of the support.

We believe the optimal temperature of boehmite precursor treatment is 800 °C. γ-Al_2O_3 support obtained under those conditions has a low concentration of strong acid sites (10.0 $\mu mol \cdot g^{-1}$) and a medium surface area (S_{BET} = 83 $m^2 \cdot g^{-1}$). A decrease of the temperature to 750 °C is accompanied by a 1.6-fold increase in the concentration of strong acid sites (up to 16.2 $\mu mol \cdot g^{-1}$) and an increase of surface area by only 9 $m^2 \cdot g^{-1}$ (up to 92 $m^2 \cdot g^{-1}$). An increase of the temperature to 850 °C leads to a decrease in the specific surface area by 21 $m^2 \cdot g^{-1}$ and a decrease in the concentration of strong acid sites by just 1.5 $\mu mol \cdot g^{-1}$ (Table 1).

2.1.2. SiO_2-Modification of the Support

SiO_2-modification of the support was carried out by its impregnation with an aqueous SiO_2-sol and subsequent thermal treatment at 800 °C. Introduction of silica in an amount of 2.5–7.5 wt % does not affect the phase composition of the support. In the X-ray diffraction patterns of all the samples (not shown in the current paper) the characteristic peaks of only γ-Al_2O_3 were identified. The absence of changes in the crystalline structure of the supports leads to the conclusion that the SiO_2 is localized on the support's surface. In the IR-spectrum of the SiO_2-modified support the absorption band of Si–OH at 3741 cm^{-1} [17,18] appears with a decrease of the intensity of the bands at 3751 and 3771 cm^{-1} (Al–OH bond vibrations [19,20]) (Figure 4). This also indicates that the SiO_2 is distributed on the support surface.
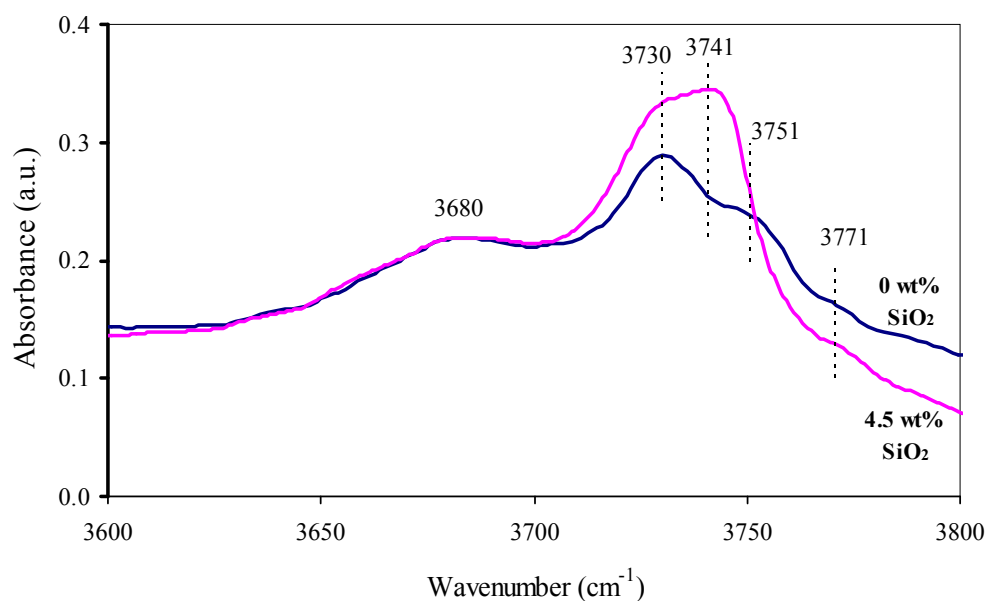

Figure 4. IR spectra of initial alumina support and a support containing 4.5 wt % SiO_2.

On the surface of the modified supports silica is distributed in the form of SiO_x-fragments $Si(OSi)_3O$ and $Si(OSi)_4$. This is indicated by the occurrence of the signals at -101 and -125 ppm on the ^{29}Si Magic Angle Spinning Nuclear Magnetic Resonance (MAS NMR) spectra (Figure 5) [18,21–24].

The distribution of the modifier on the surface leads to changes in the porous system of the supports. The volume of the pores with diameter less than 10 nm decreases from 0.08 to 0.06 $cm^3 \cdot g^{-1}$. SiO_x-islands form additional porosity in the range of diameters 10–30 nm; the volume of these pores increases from 0.13 to 0.16 $cm^3 \cdot g^{-1}$ (Figure 6). At the same time the specific surface area does not change significantly (Table 2).
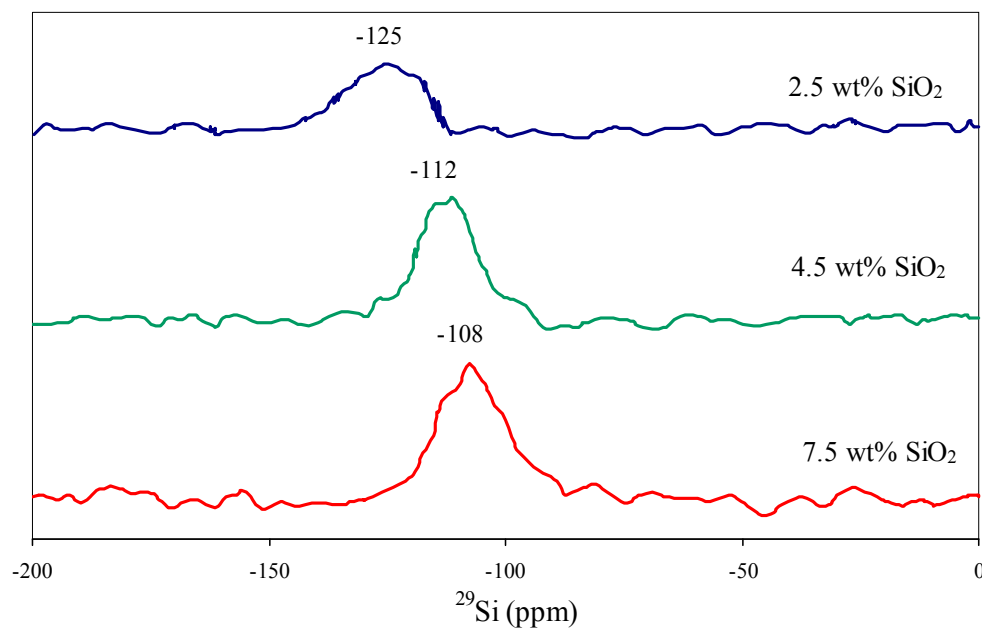
Figure 5. ^{29}Si Magic Angle Spinning Nuclear Magnetic Resonance (MAS NMR) spectra of SiO$_2$-modified supports.
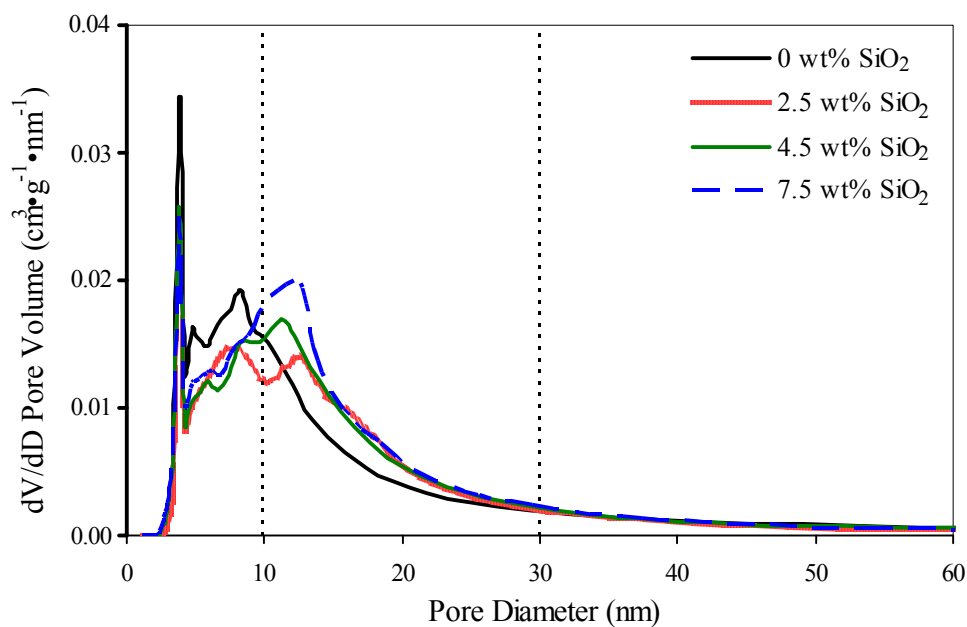

Figure 6. Pore size distribution for initial and SiO$_2$-modified supports.

Table 2. Porous system parameters of supports.

SiO$_2$ Content (wt %)	BET Surface Area (m$^2 \cdot$g^{-1})	Pore Volume (cm$^3 \cdot$g^{-1})	Distribution of Pore Volume (cm$^3 \cdot$g^{-1}) over Pore Diameters		
			<10 nm	10–30 nm	>30 nm
0	83	0.26	0.08	0.13	0.05
2.5	80	0.27	0.06	0.15	0.06
4.5	82	0.27	0.06	0.15	0.06
7.5	87	0.28	0.06	0.16	0.06

SiO$_2$-modification of the support causes changes in the surface acidity (Figure 7, Table 3). It increases from 102.3 to 109.0–125.3 µmol$\cdot$g^{-1} due to the formation of weak ($E_{\text{des.NH}_3} < 100$ kJ$\cdot$mol^{-1})

and medium ($E_{\text{des.NH}_3}$ = 100–150 kJ·mol^{-1}) acid sites (Table 3). This is indicated by the growth of the NH$_3$-TPD (temperature programmed desorption) profiles in the range 160–350 °C (Figure 7). Along with the formation of an additional amount of the weak and medium sites the concentration of strong acid sites (with $E_{\text{des.NH}_3}$ > 150 kJ·mol^{-1}) decreases (Table 3). This is indicated by the decrease in intensity of the high temperature component (400–500 °C) of the NH$_3$-TPD profile. The maximal temperature of ammonia desorption shifts to lower values (Figure 7) indicating a decrease in strength of the acid sites.
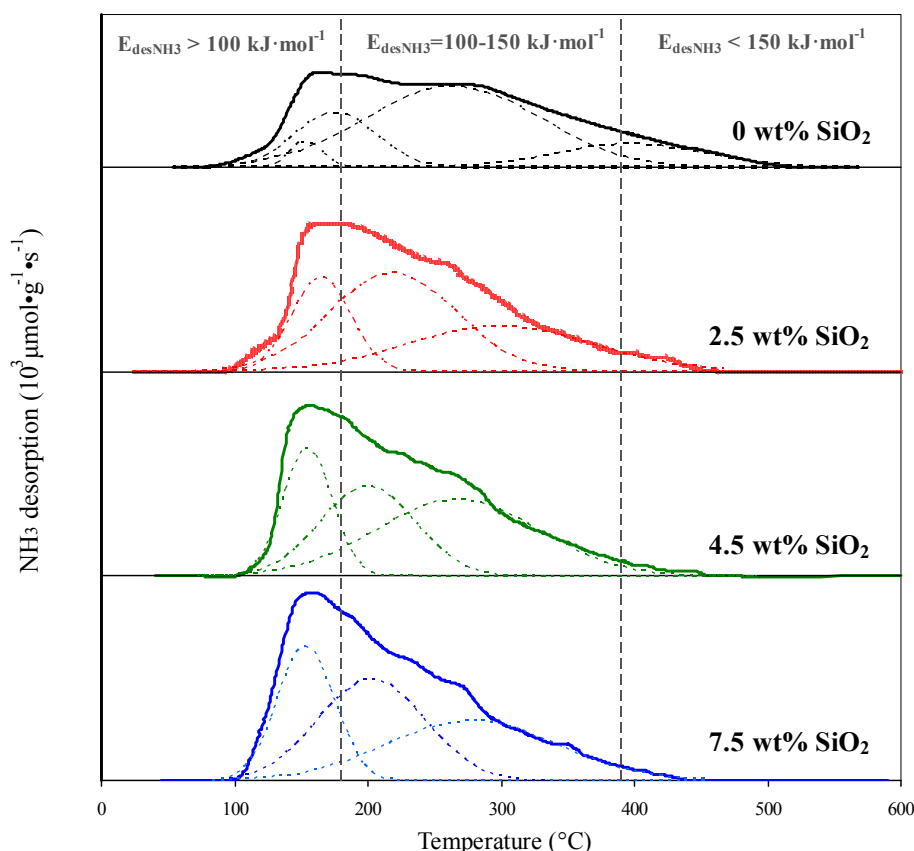

Figure 7. NH$_3$-TPD (temperature programmed desorption) patterns of initial and SiO$_2$-modified supports.

Table 3. Results from NH$_3$-TPD (temperature programmed desorption) measurement of supports.

SiO$_2$ Content (wt %)	Total Number of Acid Sites (µmol·g^{-1})	Distribution of Acid Sites (µmol·g^{-1}) on the Energy of Ammonia Desorption		
		<100 kJ·mol^{-1}	100–150 kJ·mol^{-1}	>150 kJ·mol^{-1}
0	102.3	25.6	66.7	10.0
2.5	115.2	29.0	81.8	4.5
4.5	119.4	37.5	78.7	3.1
7.5	125.3	45.0	78.0	2.4

It is likely that the acid sites formed are hydroxyl groups bonded to the silicon atoms and the Lewis acid sites of various structures [21,24]. For example, Iengo et al. [21] suggested, that the new acid sites are formed at the border of the SiO$_x$-islands, where aluminum and silicon are arranged relative to each other in such a way, that the aluminum atoms are positively charged and partially neutralized by the negative charges of the silicates. The decrease in number of the strong acid sites upon modification is probably due to them being covered by SiO$_x$-islands.

2.2. Chromia-Alumina Catalyst

2.2.1. Composition, Crystal and Pore Structure, Acidity of Catalysts

On the basis of the initial alumina support it was established that surface concentration 10 atoms·nm^{-2} provides both high activity and the absence of crystalline α-Cr_2O_3 in the catalyst (Figure 8), which accelerate catalyst sintering and decreases its thermal stability (Table 4).

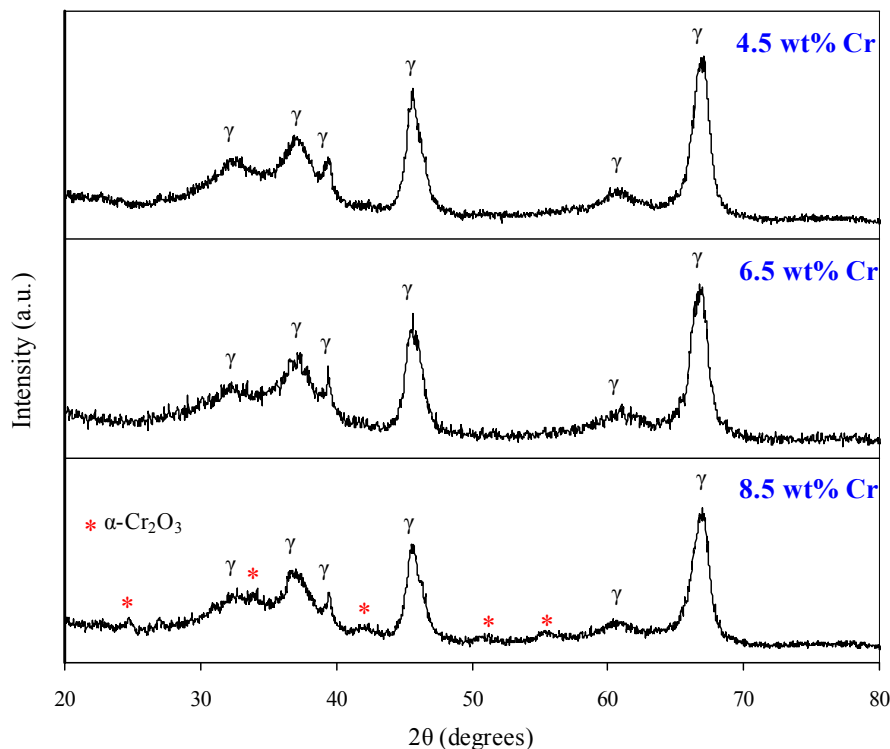**Figure 8.** X-ray diffraction patterns of catalysts.

Table 4. The composition of catalysts and their performance in isobutane dehydrogenation.

Chromium Content (wt %)	Potassium Content (wt %)	Surface Concentration of Chromium (atoms·nm^{-2})	Dehydrogenation Rate ($\mu mol_{C_4H_{10}}·g_{cat}^{-1}·s^{-1}$)		Cracking Rate ($\mu mol[C_1-C_3]·g_{cat}^{-1}·s^{-1}$)
			Initial	After Treatment at 1000 °C	Initial
4.5	0.6	6.5	2.7	2.4	0.32
6.5	0	10.0	2.8	-	0.47
6.5	0.8	10.0	3.0	3.1	0.29
8.5	1.1	13.5	3.1	2.5	0.27

In the synthesized catalysts an optimum mass ratio of chromium to potassium was used (Cr/K = 8) which was established by Kataev [25] for alumina supports obtained by the sequential thermal-hydrothermal treatment of gibbsite. Potassium as a promoter performs several functions in chromia-alumina catalysts. It neutralizes the strong acid sites [15] and thus decreases the activity of the catalyst in hydrocarbon cracking reactions (Table 4). Potassium in catalyst forms potassium chromates at the expense of the low-active crystalline Cr_2O_3 phase. These chromates are reduced to catalytically active Cr(III) phase in dehydrogenation conditions [15,26]. However, an excessive amount of potassium poisons the catalyst due to the coverage of the active Cr(III) sites [26] and neutralization of the weak and medium acid sites which adsorb alkane molecules [15]. Optimal potassium content depends not only on the surface area and acidity of the support but also on the concentration of chromium because potassium as aluminate and chromates is distributed both on the open areas of alumina and on the Cr_2O_3 particles [26].

The chromia-alumina catalysts with a surface concentration of chromium 10 atoms·nm^{-2} were synthesized on the SiO$_2$-modified supports (Table 5).

Table 5. Composition, Cr(VI) content, specific surface area and pore volume of the initial and SiO$_2$-modified catalysts.

Chromium Content (wt %)	Potassium Content (wt %)	SiO$_2$ Content (wt %)	Cr(VI) Content [1] (wt %)	BET Surface Area (m^2·g^{-1})	Pore Volume (cm^3·g^{-1})
6.5	0.8	0	2.5	77	0.22
6.5	0.8	2.5	1.9	73	0.22
6.5	0.8	4.5	1.6	74	0.22
6.5	0.8	7.5	1.4	70	0.22

[1] Cr(VI) was calculated as CrO$_3$.

As a result of the chromium and potassium distribution in the pores of initial and SiO$_2$-modified support (Figure 9), specific surface area and pore volume decrease slightly-by 6–17 m^2·g^{-1} and 0.04–0.06 cm^3·g^{-1} respectively (Tables 1 and 5).
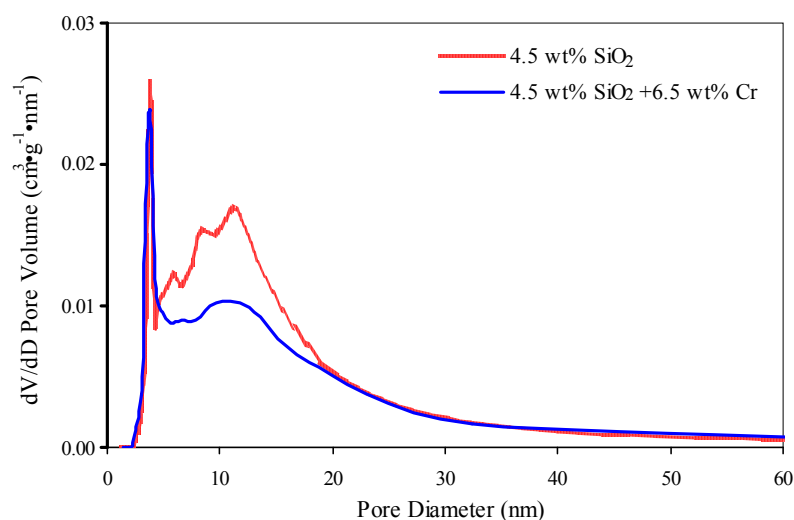

Figure 9. Pore size distribution for support with 4.5 wt % SiO$_2$ and for catalyst based on it.

Introduction of 6.5 wt % chromium and 0.8 wt % potassium to supports decreases the number of acid sites by 15.7–29.9 μmol·g^{-1} (Tables 3 and 6). SiO$_2$ affects the acidity of the catalysts similar to those of the supports: introduction of 2.5–7.5 wt % SiO$_2$ increases the total acidity of catalyst due to the formation of an additional weak and medium acid sites; it also decreases the number of strong acid sites.

Table 6. Results from NH$_3$-TPD measurement of catalysts.

SiO$_2$ Content (wt %)	Total Number of Acid Sites (μmol·g^{-1})	Distribution of Acid Sites (μmol·g^{-1}) on the Energy of Ammonia Desorption		
		<100 kJ·mol^{-1}	100–150 kJ·mol^{-1}	>150 kJ·mol^{-1}
0	72.4	9.3	53.4	9.7
2.5	93.7	12.9	78.0	2.8
4.5	102.8	15.7	85.5	1.6
7.5	109.6	13.8	95.6	0.2

2.2.2. Active Component of Catalysts

Formation on the support surface of SiO_x-islands results in changes in the distribution of the active component. Modification of the support by 2.5–7.5 wt % SiO_2 leads to a decrease of Cr(VI) content in the catalysts based on it.

By diffuse reflectance UV-Vis spectroscopy it was found that chromium deposition on the SiO_2-modified supports results in an increase of Cr(III) content in comparison to the initial support. It can be seen by the increase in intensity of the signal at ~17,000 cm^{-1} (Figure 10) which corresponds to an electronic transition $^4A_{2g} \rightarrow ^4T_{2g}$ in the $Cr(III)_{oct}$ ion [26,27]. Increasing the Cr(III) content is consistent with the data of the iodometric titration, showing that the concentration of Cr(VI) (calculated as CrO_3) decreases from 2.5 to 1.4 wt % with an increase of SiO_2 content from 0 to 7.5 wt % (Table 5). UV-Vis spectra also demonstrate a shift of the Cr(VI) signal at ~27,000 cm^{-1} [26,28,29] to the short-wavelength region and an increase in intensity of the complex Cr(III)-Cr(VI) signal at ~22,000 cm^{-1} [26–29] (Figure 10). In combination these indicate a decrease in symmetry of surface chromates due to oligomerization of Cr(VI) compounds [26].
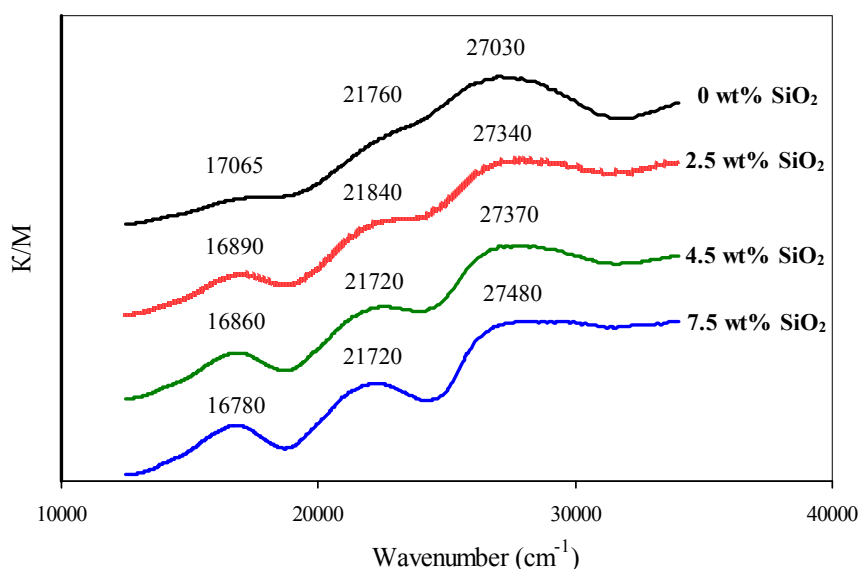

Figure 10. Diffuse reflectance UV-Vis-spectra of catalysts (6.5 wt % Cr; 0.8 wt % K).

The increase in Cr(III) content observed by UV-Vis spectroscopy and the oligomerization of surface Cr(VI) compounds are consistent with the Raman-spectroscopy data. Here, the increase in SiO_2 content results in the growth in intensity of the signal at ~550 cm^{-1}, corresponding to the vibrations of the $Cr(III)_{oct}$–O bond [26,30,31]; the intensity of hydrated dichromate signals at 906 and 948 cm^{-1} [28,30] decreases; the typical signals of dehydrated polychromates at 850–900 and 1000 cm^{-1} [28,30–32] also appear (Figure 11).

Decreasing Cr(VI) content and the simultaneous oligomerization of chromates indicates a decrease of stabilization of the chromates by the support surface through *X*–O–Cr (*X* = Al, Si) bonds. This is also supported by the temperature-programmed reduction of catalysts. All H_2-TPR profiles are decomposed into 3–4 Gaussian components which correspond to the chromates with different degrees of binding to the surface. The higher the temperature of chromate reduction the greater is the number of *X*–O–Cr bonds per one chromium atom [26,33]. Therefore, the low-temperature components (at 300–450 °C and 400–450 °C) most likely correspond to polychromates, and the high-temperature components (at 450–600 °C and 500–650 °C) correspond to mono- and dichromates. The introduction of 2.5–7.5 wt % SiO_2 leads to the redistribution of the hydrogen consumption temperature: the low temperature component of the H_2-TPR profile (in the region 300–400 °C) increases and the high temperature component (in the range 500–600 °C) decreases. The Gaussian component of the H_2-TPR profile

in the region 550–600 °C, corresponding to monochromates with the highest degree of interaction with the support surface, disappears. The maximum on the H$_2$-TPR profiles sequentially shifts from 436 to 419 °C (Figure 12).
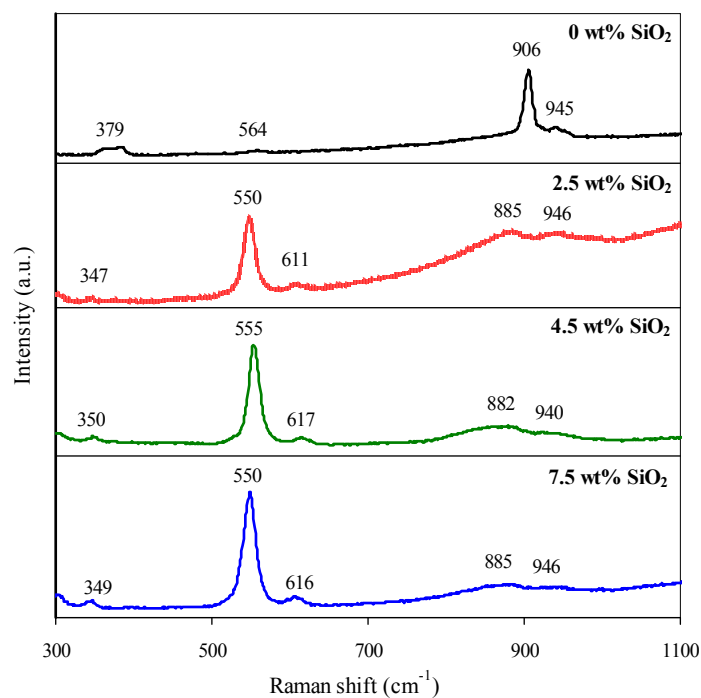

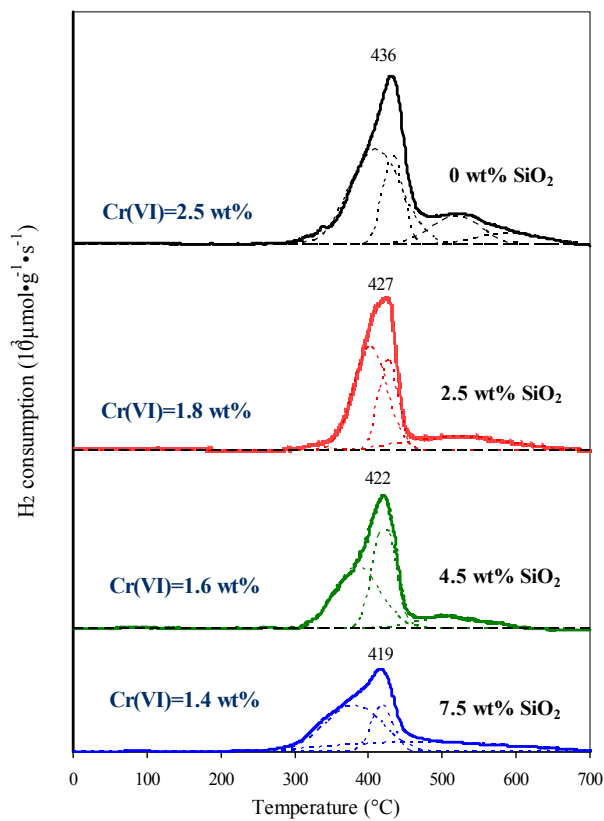**Figure 11.** Raman-spectra of catalysts.

Figure 12. H$_2$-temperature programmed reduction (TPR) profiles of catalysts.

The decrease in interaction between the support and the active component is due to the changes in hydroxyl cover of the support. The isoelectronic point (IEP) of alumina is 7.2–8.6, and the IEP of silica is 2.0–3.9 [34–36]. This is caused by the predominance of the following reactions on the surface of the hydrated supports [34,36]:

$$-\text{Al-OH} + \text{H}^+ \leftrightarrow -\text{AlOH}_2{}^+ \tag{1}$$

$$-\text{Si-OH} \leftrightarrow -\text{SiO}^- + \text{H}^+ \tag{2}$$

Due to a larger number of basic sites on the alumina surface during deposition of the active component from an aqueous solution of chromic acid and subsequent heat treatment, a greater interaction of chromate ions with Al_2O_3 rather than with SiO_2 and SiO_2–Al_2O_3 is observed [37]. The interaction of chromate ions with the alumina surface is complex [35] and consists of:

(1)   acid-base reaction between the neutral surface hydroxyl groups and chromate anions (Scheme 2):
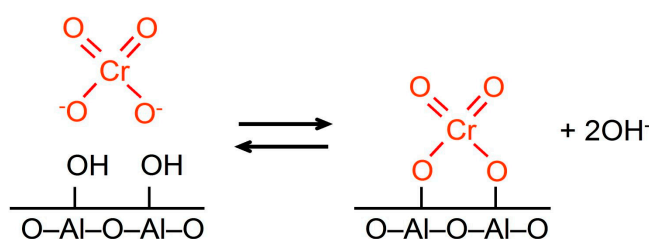
Scheme 2. Reaction between chromate ion and surface hydroxyl groups.

(2)   electrostatic attraction (Scheme 3) between the chromate ions and the positive-charged surface sites (in the inner Helmholtz plane of the electrical double layer) which is formed by protonation of the surface hydroxyl groups (Reaction (1)) [35]:
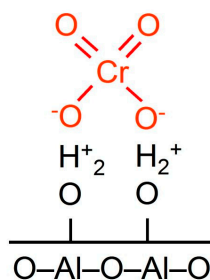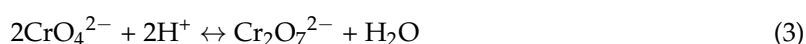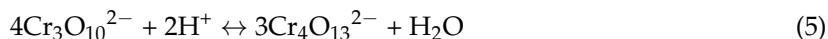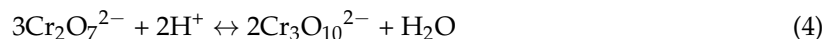

Scheme 3. Electrostatic interaction between chromate ion and positive-charged surface sites of alumina.

Therefore, on the surface of alumina predominantly mono- and dichromate anions are stabilized (Scheme 4).

As is shown the formation of SiO_x-islands on the alumina surface leads to diminution in interaction between Cr(VI) compounds and the support. It may occur due to the following reasons:

–   decrease in the number of surface basic hydroxyls capable of acid-base reaction (Scheme 2) with chromate ions;
– SiO_2 introduction results in a drop of the pH of the electrical double layer. This in turn leads to a shift of the equilibrium of Reactions (3)–(5) to the right, towards formation of polynuclear chromate ions [31].

$$2\text{CrO}_4{}^{2-} + 2\text{H}^+ \leftrightarrow \text{Cr}_2\text{O}_7{}^{2-} + \text{H}_2\text{O} \tag{3}$$

$$3Cr_2O_7{}^{2-} + 2H^+ \leftrightarrow 2Cr_3O_{10}{}^{2-} + H_2O \tag{4}$$

$$4Cr_3O_{10}{}^{2-} + 2H^+ \leftrightarrow 3Cr_4O_{13}{}^{2-} + H_2O \tag{5}$$

−   according to Reaction (2) the part of the inner Helmholtz plane becomes negatively charged which results in the electrostatic attraction between support surface and chromate ions diminishing.

A decrease in the number of Cr–O–*X* (*X* = Al, Si) bonds leads to the stabilization of the polychromate ions and polynuclear [–Cr(III)–O–Cr(III)–]$_n$ ions (also called amorphous Cr$_2$O$_3$ [26] or Cr$_2$O$_3$-clusters [28]) (Scheme 4) by the SiO$_2$-modified support surface after thermal activation of the catalyst. A similar effect of SiO$_2$ has also been reported by Weckhuysen et al. [29]; at the transition from Al$_2$O$_3$ to aluminosilicate (with 40 wt % SiO$_2$) the chromate/dichromate band intensity ratio on the UV-Vis spectra of the samples calcined at 550 °C decreased from ∞ to 2.18. Weckhuysen et al. [38] reported that in SiO$_2$ with 0.2 wt % Cr calcined at 720 °C, Cr(III) ions were identified by UV-Vis spectroscopy, whereas for the same amount of chromium on alumina, Cr(III) ions were not observed.
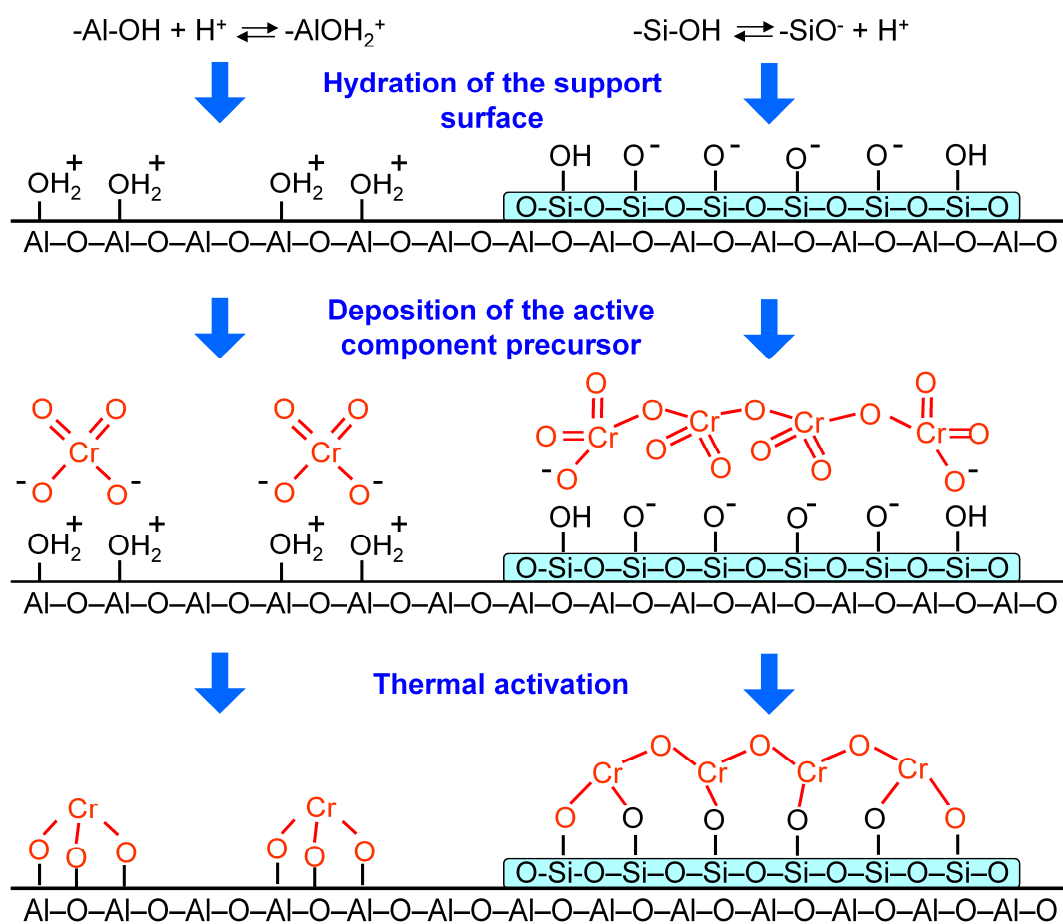
Scheme 4. Hydration of alumina and silica surface, their interaction with chromate ions.

Increasing interaction between Cr(III) ions was also confirmed by EPR-spectroscopy. Upon introduction of SiO$_2$ the intensity of the δ-signal component at *g* = 3.8–4.0, corresponding to isolated Cr(III) ions [39], decreases while the intensity of β-signal with *g* = 1.98 and Δ*H* = 1400–1600 G, corresponding to magnetically concentrated Cr(III) ions [28,39], increases (Figure 13).
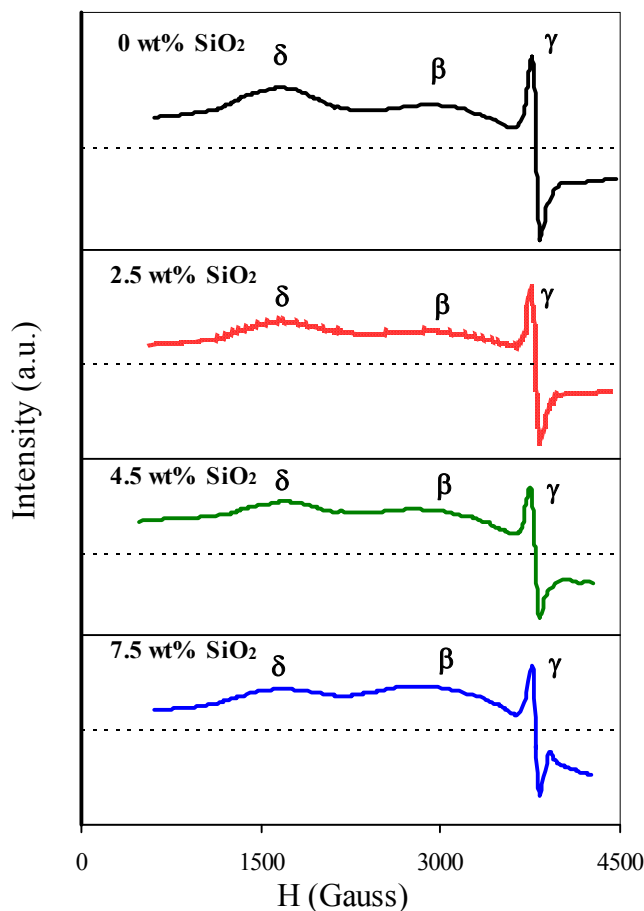
Figure 13. Electron paramagnetic resonance (EPR) spectra of catalysts.

### 2.2.3. Isobutane Dehydrogenation Performance of Catalysts

Chromia-alumina catalysts were tested in isobutane dehydrogenation at 570 °C. The curves of dehydrogenation and cracking rate versus time on stream are shown on Figure 14a,b, respectively. All the curves on Figure 14a show the maxima as a function of time on stream. In all the cases at the initial stage of the dehydrogenation cycle (for the first 30–55 min) an increase of catalyst dehydrogenation activity by 8%–9.5% is observed (Figure 14a); this is the catalyst development period. As we know [40,41] during catalyst development the surface stabilized Cr(VI) compounds are reduced by hydrocarbons to additional catalytically active Cr(III) compounds. Decrease of the dehydrogenation rate at the final stage of the cycle is due to the catalyst coking. The decrease of the cracking rate during the first 30 min (Figure 14b) is also caused by covering of the acid sites by coke deposits [15].

The increase in the content of amorphous Cr_2O_3 phase, which is the most active in the dehydrogenation of light alkanes [26], and the formation of polychromates which also reduce to amorphous Cr_2O_3, causes an increase in dehydrogenation activity of catalysts based on SiO_2-modified supports (Figure 14a). The average dehydrogenation activity increases by 10%–14%—from 2.9 to 3.2–3.3 µmol $C_4H_{10} \cdot g_{cat}^{-1} \cdot s^{-1}$. At the same time the catalyst development period diminishes due to a decrease in the Cr(VI) content. The rise in dehydrogenation activity with the increase in the polynuclear Cr(III) ions content is consistent with the results of the kinetic studies by Airaksinen et al. [42] and Carra et al [43]. According to these works the dehydrogenation of one molecule of butane proceeds at two active sites.

A decrease in the number of strong acid sites upon SiO_2-modification of support leads to a decrease in cracking rate on catalysts with 2.5–7.5 wt % SiO_2 (Figure 14b). The average cracking rate decreases by 18%–34%—from 0.29 to 0.19–0.24 µmol $(C_1–C_3) \cdot g_{cat}^{-1} \cdot s^{-1}$.
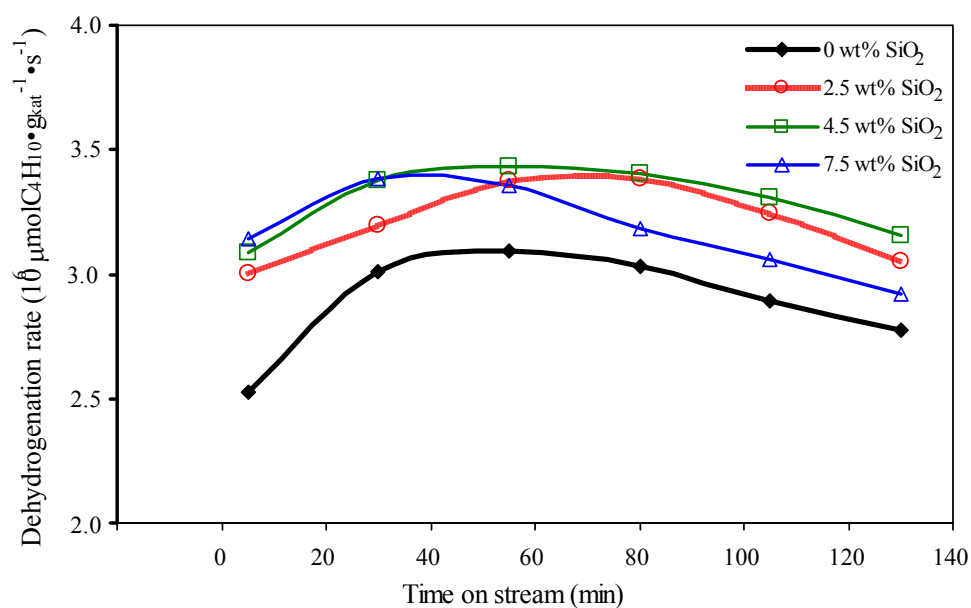
(**a**)
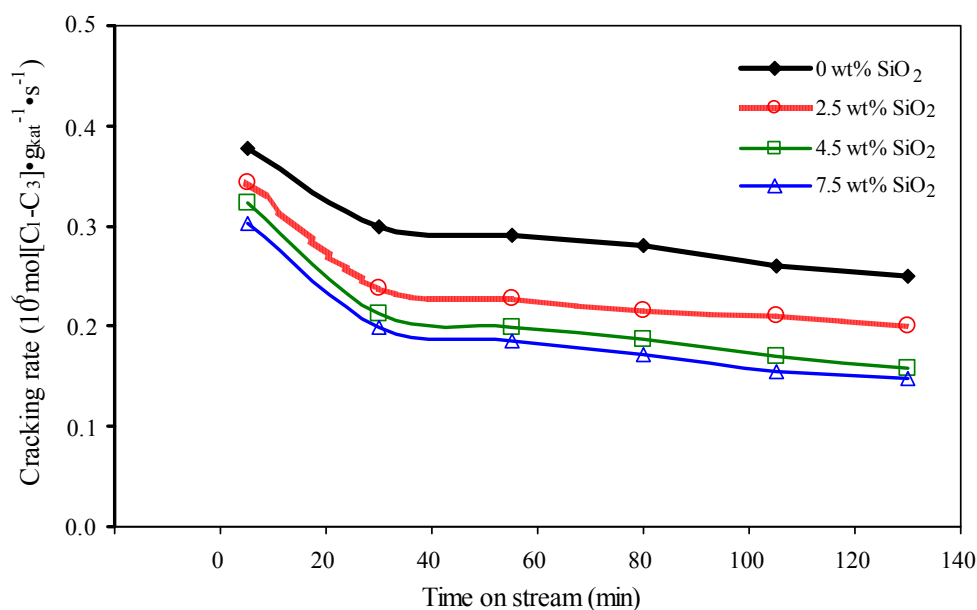
(**b**)

Figure 14. Dehydrogenation rate (**a**) and cracking rate (**b**) versus time on stream.

3. Materials and Methods

3.1. Preparation of Supports and Catalysts

Microspherical (40–200 μm) boehmite support prepared by consecutive thermal and hydrothermal treatment of aluminum trihydroxide (GD00 grade, produced by Bogoslovsk Aluminum Smelter, Krasnoturyinsk city, Russia) under industrial conditions [11] in an autoclave for 3 h at 195 °C (Chemical Plant Karpov, Mendeleyevsk city, Russia), was used for the synthesis of alumina supports and chromia-alumina catalysts. According to thermogravimetry the phase composition of the support precursor is the following: boehmite—96.0 wt %, gibbsite—3.0 wt%, Al_2O_3—1.0 wt %.

SiO_2 was introduced into the support by incipient wetness impregnation with a water silica sol ("Leiksil" brand produced by "Compas" Scientific and Technical Center, Kazan city, Russia).

The catalyst was prepared by incipient wetness impregnation of the support with an aqueous solution of chromic acid and potassium carbonate, followed by drying under vacuum. Then the catalyst was activated by thermal treatment in a muffle furnace at 750 °C for 4 h.

3.2. Characterization of Supports and Catalysts

Thermogravimetric analysis was performed with a STA-449C (Netzsch, Selb, Germany) combined thermogravimetric and differential scanning calorimetric (DSC) analyzer coupled with an Aeolos QMS 403 quadruple mass spectrometer (Netzsch, Selb, Germany) in a temperature range of 30–1000 °C at a heating rate of 10 °C. min^{-1} in a flow of argon. The concentrations of aluminum hydroxide phases were calculated from the amount of water released in their dehydration.

Scanning electron microscopy was performed on an EVO 50 XVP (Carl Zeiss, Oberkochen, Germany) electron microscope.

The elemental composition of the catalysts was determined by X-ray fluorescence spectroscopy on a Clever C31 instrument (ELERAN, Elektrostal, Russia).

Powder X-ray diffraction measurements were carried out using a DRON-2 diffractometer (Burevestnik, Saint Petersburg, Russia). The patterns were obtained using CuKα radiation and graphite monochromator (λ = 1.54187 Å) at 30 kV and 15 mA. The identification of different crystalline phases in the samples was performed by comparing the data with the Joint Committee for Powder Diffraction Standards (JCPDS) files. The crystallite size of the boehmite phase was calculated using the Selyakov–Scherrer Equation. The error in determining the crystallite size was 10%.

Specific surface (S_{sp}) and pore volume (V_p) of samples were determined from the N_2 physisorption measurements at 196 °C using an universal Autosorb-iQ analyzer (Quantachrome, Boynton Beach, FL, USA). Prior to measurement, the sample was outgassed for 1 h at 150 °C (for boehmite precursor) or for 3 h at 300 °C (for alumina supports and catalysts). S_{sp} and V_p were calculated according to the Brunauer-Emmett-Teller method. The pore diameter distribution was calculated by the desorption branch of isotherm using the standard Barrett–Joyner–Halenda method.

The ^{29}Si MAS NMR spectra of supports were recorded at room temperature on an Avance 400 spectrometer (Bruker, Ettlingen, Germany) operating at frequencies of 79.5 MHz with spectral resolution 48.83 Hz. The sample rotation frequency was 5 kHz.

The IR spectra of supports were measured on a VERTEX 70 (Bruker, Ettlingen, Germany) instrument fitted with a mercury−cadmium−telluride detector. The measurements were done in transmission mode using a Harrick high temperature cell. A background spectrum and the spectra were measured at 480 °C and a residual pressure of less than 10^{-3} mbar with a resolution of 1 cm^{-1} and averaged by 128 scans. For the IR analysis, samples were prepared in a tablet-shape of 20 mg; optical density was 20 mg·cm^{-2}.

Hexavalent chromium concentration in the catalyst was determined by dissolution of Cr(VI) in sulfuric acid and subsequent volumetric titration with the iodometric method.

UV-Vis diffuse reflectance spectra of the catalysts were recorded using a V-650 spectrophotometer (Jasco, Tokyo, Japan) equipped with an integrating sphere ISV-722 (Jasco, Tokyo, Japan). A $BaSO_4$ plate was used as the reference. Spectra were recorded in the wavenumber range 12,500–50,000 cm^{-1} with the spectral resolution 2 nm. UV-Vis-spectra were deconvoluted into Gaussian bands to determine the positions and intensities of the bands' maximums.

Raman spectra of catalysts were recorded using a dispersion Raman-microspectrophotometer Nicolet Almega XR (Thermo Fisher Scientific, Waltham, MA, USA). The 532 nm line of a Nd-YAG laser was used as an excitation. The spectra were recorded in the wavenumber range 100–1100 cm^{-1} with the spectral resolution 2 cm^{-1}. Each spectrum was received by averaging 10 exposures on 10 s.

EPR measurements were made at the temperature of −196 °C on a RE-1306 EPR-spectrometer (Institute of Analytical Instrumentation of Russian Academy of Sciences, Saint Petersburg, Russia)

with a working frequency 9.37 GHz and 100 kHz magnetic field modulation. Diphenylpicrylhydrazyl (g = 2.0036) was used as reference for g-value determination.

NH$_3$-TPD and H$_2$-TPR measurements were carried out on the ChemBET Pulsar TPR/TPD (Quantachrome, Boynton Beach, FL, USA). Before NH$_3$-TPD measurement the sample was degassed at 600 °C for 2 h in a helium flow. The adsorption step is carried out in an ammonia flow at 100 °C for 30 min. Then the physically sorbed ammonia was removed with helium at 100 °C for 30 min and the sample was cooled to a room temperature in the helium flow. Temperature programmed desorption was performed from room temperature to 700 °C at a heating rate of 10 °C·min^{-1}. The strength of the acid sites was evaluated by the temperature of ammonia desorption [44]. A temperature of 175 °C corresponds to ammonia desorption energy of 100 kJ·mol^{-1} and a temperature of 380 °C to the desorption energy 150 kJ·mol^{-1}. Acid sites with ammonia desorption energy lower than 100 kJ·mol^{-1} were attributed to weak ones, while the sites with desorption energies of 100–150 kJ·mol^{-1} and higher than 150 kJ·mol^{-1} were attributed to medium and strong sites respectively. The number of weak, medium and strong acid sites was calculated from the area under the NH$_3$-TPD profiles in the temperature ranges <175 °C, 175–380 °C and >380 °C respectively.

Before H$_2$-TPR measurement the catalyst was heated to 650 °C and held at this temperature for 60 min in a flow of a gas mixture (5 vol% O$_2$ + 95 vol% N$_2$). Then the catalyst was cooled down to room temperature in the helium flow. Temperature programmed reduction was performed from room temperature to 700 °C at a heating rate of 10 °C·min^{-1}. NH$_3$-TPD and H$_2$-TPR profiles were Gauss fitted using the TPRWin software (version 3.52, Quantachrome, Boynton Beach, FL, USA, 2012).

3.3. Catalyst Testing

The catalysts were tested in the reaction of isobutane dehydrogenation in a steel fixed bed reactor of 10 mm internal diameter under atmospheric pressure. An amount of 2 g of fresh catalyst (sieve fraction 40–200 μm) was filled into the reactor. The catalyst was heated at 5 °C·min^{-1} to 650 °C in an air flow (60 mL·min^{-1}) followed by flushing with air for 30 min at the same temperature. The catalyst was cooled in air to 570 °C and flushed with argon for 15 min at that temperature. Then a mixture of 30 vol% C$_4$H$_{10}$ in Ar was fed at a rate of 60 mL·min^{-1} at the same reaction temperature. The reaction was run for 130 min followed by catalyst regeneration in an air flow for 60 min at 650 °C. The regeneration/dehydrogenation cycles were repeated three times.

The hydrocarbon composition of feed and reaction products were analyzed by gas chromatography on a GH-1000 instrument (Chromos, Dzerzhinsk, Russia) with a flame-ionization detector and a capillary VP-Alumina/KCl column (VICI Valco, Houston, TX, USA). The concentrations of H$_2$, CH$_4$, and CO were determined with the use of a column filled by 13× molecular sieves on a GH-1000 apparatus with a thermal conductivity detector.

Based on of the results of chromatographic analysis the rates of i-C$_4$H$_{10}$ dehydrogenation and cracking of hydrocarbons were calculated using Equations (6) and (7), respectively.

$$\text{Dehydrogenation Rate} = \frac{X(\text{iC}_4\text{H}_{10}) \times F}{3600 \times 100 \times m_{\text{cat}}} \tag{6}$$

$$\text{Cracking Rate} = \frac{(C_{\text{CH}_4} + C_{\text{C}_2\text{H}_6} + C_{\text{C}_2\text{H}_4} + C_{\text{C}_3\text{H}_8} + C_{\text{C}_3H_6}) \cdot V^{\text{outlet}}}{22400 \cdot 3600 \cdot 100 \cdot m_{\text{cat}}} \tag{7}$$

where $X(\text{iC}_4\text{H}_{10})$ is the isobutane conversion, %; F is the feed rate of isobutane, mole·h^{-1}; m_{cat} is the weight of catalyst, g; C_{CH_4}, $C_{\text{C}_2\text{H}_6}$, $C_{\text{C}_2\text{H}_4}$, $C_{\text{C}_3\text{H}_8}$, $C_{\text{C}_3\text{H}_6}$ are the concentrations of methane, ethane, ethylene, propane, propylene respectively in the reaction products, vol%; V^{outlet} is the volumetric flow of the reaction products, mL·h^{-1}.

4. Conclusions

The distribution of SiO$_2$ and its effect on the structure and acidity of the alumina support, as well as the effect of SiO$_2$ on the active component and the performance in isobutane dehydrogenation of

chromia-alumina catalyst were investigated. It was shown that SiO_2 in an amount of 2.5–7.5 wt % is distributed on the surface of alumina in the form of $Si(OSi)_4$ and $Si(OSi)_3(O–)$ compounds. These SiO_x-islands on the support produce additional porosity with a pore range 10–30 nm, as well as additional weak and medium acid sites. At the same time SiO_2-modification causes a decrease in the number of strong acid sites.

Upon introduction of the active component, the SiO_x-islands diminish the interaction of chromate ions with the support surface; as a consequence polychromates are the compounds predominantly stabilized on the support. During thermal activation of the catalyst these polychromates are reduced to a phase of amorphous Cr_2O_3. This results in the increase of the catalyst activity in the isobutane dehydrogenation. At the same time, the decrease in the number of strong acid sites in SiO_2-modified catalysts leads to a diminution of its activity in hydrocarbon cracking reactions.

Author Contributions: S.R.E and A.A.L conceived and designed the experiments; G.E.B. and A.N.M. performed the experiments. All authors participated in the analysis of the data and writing of the paper. G.E.B., A.N.M. and S.R.E. proofread the manuscript.

Conflicts of Interest: The authors declare no conflict of interest.

References

1. Voloshina, O.A.; Nazarova, E.A.; Petrov, I.M. *Obzor Rynka Promyshlennyh Katalyzatorov v Rossii (Review of Industrial Catalyst's Market in Russia)*; INFOMINE Research Group: Moscow, Russia, 2008; pp. 213–218.
2. Sattler, J.J.H.B.; Ruiz-Martinez, J.; Santillan-Jimenez, E.; Weckhuysen, B.M. Catalytic dehydrogenation of light alkanes on metals and metal oxides. *Chem. Rev.* **2014**, *114*, 10613–10653. [CrossRef] [PubMed]
3. Kolesnikov, I.M. *Kataliz i Proizvodstvo Katalizatorov (Catalysis and Catalysts Production)*; Tehnika: Moscow, Russia, 2004; pp. 314–315.
4. Pakhomov, N.A.; Parakhin, O.A.; Nemykina, E.I.; Danilevich, V.V.; Chernov, M.P.; Pecherichenko, V.A. Microspherical chromium oxide/alumina catalyst KDM for fluidized bed isobutane dehydrogenation: Development and industrial application experience. *Catal. Ind.* **2012**, *4*, 298–307. [CrossRef]
5. Egorova, S.R.; Kataev, A.N.; Bekmukhamedov, G.E.; Lamberov, A.A.; Gil'mullin, R.R.; Nesterov, O.N. Development of technology for the production of microspherical aluminum oxide supporter for the paraffin dehydrogenation catalyst. *Catal. Ind.* **2009**, *1*, 381–390. [CrossRef]
6. Zeeshan, N. Light alkane dehydrogenation to light olefin technologies: A comprehensive review. *Rev. Chem. Eng.* **2015**, *31*, 413–436.
7. Sanfilippo, D.; Miracca, I. Dehydrogenation of paraffins: synergies between catalyst design and reactor engineering. *Catal. Today* **2006**, *111*, 133–139. [CrossRef]
8. Korhonen, S.T.; Airaksinen, S.M.K.; Banares, M.A.; Krause, A.O.I. Isobutane dehydrogenation on zirconia-, alumina-, and zirconia/alumina-supported chromia catalysts. *Appl. Catal. A* **2007**, *333*, 30–41. [CrossRef]
9. Bugrova, T.A.; Litvyakova, N.N.; Mamontov, G.V. Effect of zirconia additives on the activity of the Cr/SiO_2 catalyst in isobutane dehydrogenation. *Kinet. Catal.* **2015**, *56*, 758–763. [CrossRef]
10. Jiménez-López, A.; Rodr'ıguez-Castellón, E.; Maireles-Torres, P.; D'ıaz, L.; Mérida-Robles, J. Chromium oxide supported on zirconium- and lanthanum-doped mesoporous silica for oxidative dehydrogenation of propane. *Appl. Catal. A* **2001**, *218*, 295–306. [CrossRef]
11. Hoang, D.L.; Dittmar, A.; Radnik, J.; Brzezinka, K.-W.; Witke, K. Redox behaviour of La-Cr compounds formed in CrO_x/La_2O_3 mixed oxides and $CrO_x/La_2O_3/ZrO_2$ catalysts. *Appl. Catal. A* **2003**, *239*, 95–110. [CrossRef]
12. Cabrera, F.; Ardissone, D.; Gorriz, O.F. Dehydrogenation of propane on chromia/alumina catalysts promoted by tin. *Catal. Today* **2008**, *133–135*, 800–804. [CrossRef]
13. Babenko, V.S.; Pakhomov, N.A.; Buyanov, R.A. Investigation of the thermal stability of the chromia–alumina catalysts for the process of the one-stage dehydrogenation of *n*-butane. *Catal. Ind.* **2009**, *1*, 43–49. [CrossRef]
14. Buonomo, F.; Jezzi, R.; Notari, B.; Kotelnikov, G.R.; Michailov, K.R.; Patanov, V.A. Method for the Preparation of a Catalyst for the Dehydrogenation of C_3-C_5 paraffins. U.S. Patent 4746643, 24 May 1988.

15. Rombi, E.; Cutrufello, M.G.; Solinas, V.; De Rossi, S.; Ferraris, G.; Pistone, A. Effects of potassium addition on the acidity and reducibility of chromia/alumina dehydrogenation catalysts. *Appl. Catal. A* **2003**, *251*, 255–266. [CrossRef]

16. Paukshtis, E.A. *Infrakrasnaya Spectroscopya v Geterogennom Kislotno-Osnovnom Katalize (IR-spectroscopy in Heterogeneous Acid-Base Catalysis)*; Nauka: Novosibirsk, Russia, 1992; pp. 78–92.

17. Morrow, B.A.; Cody, I.A. Infrared studies of reactions on oxide surfaces. 6. Active sites on dehydroxylated silica for the chemisorption of ammonia and water. *J. Phys. Chem.* **1976**, *80*, 1998–2004. [CrossRef]

18. Lindblad, M.; Root, A. Atomically controlled preparation of silica on alumina. *Stud. Surf. Sci. Catal.* **1998**, *118*, 817–826.

19. Lundie, D.T.; McInroy, A.R.; Marshall, R.; Winfield, J.M.; Jones, P.; Dudman, C.C.; Parker, S.F.; Mitchell, C.; Lennon, D. Improved description of the surface acidity of η-alumina. *J. Phys. Chem. B.* **2005**, *109*, 11592–11601. [CrossRef] [PubMed]

20. Srinivasan, S.; Narayanan, C.R.; Datye, A.K. The role of sodium and structure on the catalytic behavior of alumina: II. IR spectroscopy. *Appl. Catal. A* **1995**, *132*, 289–308. [CrossRef]

21. Iengo, P.; Di Serio, M.; Solinas, V.; Gazzoli, D.; Salvio, G.; Santacesaria, E. Preparation and properties of new acid catalysts obtained by grafting alkoxides and derivatives on the most common supports. Part II: Grafting zirconium and silicon alkoxides on γ-alumina. *Appl. Catal. A* **1998**, *170*, 225–244. [CrossRef]

22. McMillan, M.A.; Brinen, J.S.; Carruhers, J.D.; Haller, G.L. ^{29}Si NMR investigation of the structure of amorphous silica-alumina supports. *Colloids Surf.* **1989**, *38*, 133–148. [CrossRef]

23. Sato, S.; Sodesawa, T.; Nozaki, F.; Shoji, H. Solid-state NMR of silica-alumina prepared by chemical vapor deposition. *J. Mol. Catal.* **1991**, *66*, 343–355. [CrossRef]

24. Finocchio, E.; Busca, G.; Rossini, S.; Cornaro, U.; Piccoli, V.; Miglio, R. FT-IR characterization of silicated aluminas, active olefin skeletal isomerization catalysts. *Catal. Today* **1997**, *33*, 335–352. [CrossRef]

25. Kataev, A.N. Formation of a Monophase Microspherical Alumina Support and a Catalyst for Isobutane Dehydrogenation in the Industrial Synthesis. Ph.D. Thesis, Kazan State Technological University, Kazan, Russia, 2009; p. 106.

26. Cavani, F.; Koutyrev, M.; Trifiro, F.; Bartolini, A.; Ghisletti, D.; Iezzi, R.; Santucci, A.; Del Piero, G. Chemical and physical characterization of alumina-supported chromia-based catalysts and their activity in dehydrogenation of isobutane. *J. Catal.* **1996**, *158*, 236–250. [CrossRef]

27. Reinen, D. Ligand-field spectroscopy and chemical bonding in Cr^{3+}-containing oxidic solids. *Struct. Bond.* **1969**, *6*, 30–51.

28. Weckhuysen, B.M.; Wachs, I.E.; Schoonheyd, R.A. Surface chemistry and spectroscopy of chromium in inorganic oxides. *Chem. Rev.* **1996**, *96*, 3327–3349. [CrossRef] [PubMed]

29. Weckhuysen, B.M.; De Ridder, L.M.; Schoonheydt, R.A. A quantitative diffuse reflectance spectroscopy study of supported chromium catalysts. *J. Phys. Chem.* **1993**, *97*, 4756–4763. [CrossRef]

30. Vuurman, M.A.; Hardcastle, F.D.; Wachs, I.E. Characterization of CrO_3/Al_2O_3 catalysts under ambient conditions: influence of coverage and calcination temperature. *J. Mol. Catal.* **1993**, *84*, 193–205. [CrossRef]

31. Vuurman, M.A.; Stufkens, D.J.; Oskam, A. Raman spectra of chromium oxide species in CrO_3/Al_2O_3 catalysts. *J. Mol. Catal.* **1990**, *60*, 83–98. [CrossRef]

32. Mentasty, L.R.; Gorriz, O.F.; Cadus, L.E. Chromium oxide supported on different Al_2O_3 supports: Catalytic propane dehydrogenation. *Ind. Eng. Chem. Res.* **1999**, *38*, 396–404. [CrossRef]

33. Kanervo, J.M.; Krause, A.O.I. Characterisation of supported chromium oxide catalysts by kinetic analysis of H_2-TPR data. *J. Catal.* **2002**, *207*, 57–65. [CrossRef]

34. Parks, G.A. The isoelectric points of solid oxides, solid hydroxides and aqueous hydroxo-complex systems. *Chem. Rev.* **1965**, *65*, 177–198. [CrossRef]

35. Spanos, N.; Slavov, S.; Kordulis, Ch.; Lycourghiotis, A. Mechanism of deposition of the $CrO_4{}^{2-}$, $HCrO_4{}^-$, and $Cr_2O_7{}^{2-}$ ions on the γ-alumina surface. *Langmuir* **1994**, *10*, 3134–3147. [CrossRef]

36. Anderson, J.R. *Structura Metallicheskih Katalizatorov (Structure of Metallic Catalysts)*; Mir: Moscow, Russia, 1978; pp. 40–46.

37. Weckhuysen, B.M.; De Ridder, L.M.; Grobet, R.J.; Schoonheydt, R.A. Redox behavior and dispersion of supported chromium catalysts. *J. Phys. Chem.* **1995**, *99*, 320–326. [CrossRef]

38. Weckhuysen, B.M.; Verberckmoes, A.A.; Buttiens, A.L.; Schoonheydt, R.A. Diffuse reflectance spectroscopy study of the thermal genesis and molecular structure of chromium-supported catalysts. *J. Phys. Chem.* **1994**, *98*, 579–584. [CrossRef]

39. Puurunen, R.L.; Weckhuysen, B.M. Spectroscopic study on the irreversible deactivation of chromia/alumina dehydrogenation catalysts. *J. Catal.* **2002**, *210*, 418–430. [CrossRef]

40. Weckhuysen, B.M.; Verberckmoes, A.A.; Debaere, J.; Ooms, K.; Langhans, I.; Schoonheydt, R.A. In situ UV-Vis diffuse reflectance spectroscopy—On line activity measurements of supported chromium oxide catalysts: relating isobutane dehydrogenation activity with Cr-speciation via experimental design. *J. Mol. Catal. A Chem.* **2000**, *151*, 115–131. [CrossRef]

41. Weckhuysen, B.M.; Bensalem, A.; Schoonheydt, R.A. In situ UV-VIS diffuse reflectance spectroscopy-on-line activity measurements. Significance of Cr^{n+} species (n = 2, 3 and 6) in n-butane dehydrogenation catalyzed by supported chromium oxide catalysts. *J. Chem. Soc. Faraday Trans.* **1998**, *94*, 2011–2014. [CrossRef]

42. Airaksinen, S.M.K.; Harlin, M.E.; Krause, A.O.I. Kinetic modeling of dehydrogenation of isobutane on chromia/alumina catalyst. *Ind. Eng. Chem. Res.* **2002**, *41*, 5619–5626. [CrossRef]

43. Carrà, S.; Forni, L.; Vintani, C. Kinetics and mechanism in catalytic dehydrogenation of n-butane over chromia-alumina. *J. Catal.* **1967**, *9*, 154–165. [CrossRef]

44. Yushchenko, V.V. Calculation of the acidity spectra of catalysts from temperature-programmed ammonia desorption data. *J. Phys. Chem. (Zhurnal Fizicheskoi Khimii)* **1997**, *71*, 628–632.